Experimental observation of a mode-1 instability driven by Landau cavities in a storage ring

F. J. Cullinan⊙,* Å. Andersson, J. Breunlin, M. Brosi⊙, and P. F. Tavares

MAX IV Laboratory, Lund University, SE-22100 Lund, Sweden

Landau cavities used to lengthen the bunches in storage rings necessarily constitute a significant impedance. Because of the particular phase of the field required for bunch lengthening, they are often detuned quite considerably from resonance, more so than the main cavities. As a result, their impedance can excite the first coupled-bunch mode such that it becomes unstable. This phenomenon has previously been predicted [M. Venturini, Phys. Rev. Accel. Beams **21**, 114404 (2018)] and characterized in simulations [T. He, Phys. Rev. Accel. Beams **25**, 024401 (2022)] but experimental observation is yet to be documented. In this paper, the experimental observation of coupled-bunch modes-±1 excited by the Landau and main cavities in a fourth-generation light-source storage ring is presented. Features of the instability such as amplitude and coherent frequency at saturation have been measured and its dependency on the main rf voltage has been explored. The impact of a parked main cavity has also been investigated.

I. INTRODUCTION

Landau cavities (LCs, also known as harmonic cavities or higher-harmonic cavities) are used in many light-source storage rings to lengthen the electron bunches. Their usage is particularly common in the latest fourth generation of such rings where they are relied upon to increase the Touschek lifetime and reduce the emittance blow-up due to intrabeam scattering. They can either be passive cavities loaded by the beam itself or active cavities with an input power coupler. In both cases, they constitute a large impedance in the ring.

A common configuration for running Landau cavities is so that their fields just cancel the slope of the rf voltage at equilibrium phase, the phase at which a particle gains as much energy from the rf system as it loses to synchrotron radiation. This condition is referred to here as the flat-potential condition and Appendix A outlines how to obtain this condition with passive cavities. The slope of the rf voltage can also be canceled such that not just the first derivative of the total voltage but also the second derivative become zero. The bunches are then contained in a quartic potential, which is described in detail in [1]. If only the first derivative is zero, the equilibrium phase is at a local maximum or minimum and is actually unstable and there exists a second equilibrium phase that is stable. In all cases,

the flat-potential condition marks the boundary between lengthened bunches (with a single equilibrium phase) and overstretched bunches (with two stable equilibrium phases). For a fixed main-rf voltage and energy loss to synchrotron radiation, the Landau voltage at flat potential is practically independent of the beam current.

The larger the total R/Q of the cavities, the larger their detuning from resonance at which the flat-potential condition is satisfied for a given beam current and main-cavity (MC) voltage. If the detuning is too large then the impedance at the first revolution harmonic will be enough to excite a coupled-bunch instability (mode +1). This was already predicted by Bosch [2] and Venturini [3] and has recently been explored further in simulation [4].

The higher the beam current and the lower the main-cavity voltage, the more likely it is that mode +1 is unstable [4]. A lower quality factor for the same R/Q is also worse in these terms because it increases the impedance overlap at the first revolution harmonic. All things being otherwise equal, active Landau-cavity systems are able to achieve flat-potential conditions with a lower shunt impedance (and therefore R/Q) than passive systems thanks to their external power source. The detuning of the cavity that minimizes the required input power is also smaller than the detuning of a passive cavity, approaching the same value if the shunt impedance and beam current are both large enough that no input power is required [5,6]. However, other arguments exist for having a high shunt impedance, regardless of whether the LCs are active or passive. These include better Robinson stability [1,3] and less demanding cavity cooling if the power consumption is spread over multiple cavities.

---

*francis.cullinan@maxiv.lu.se
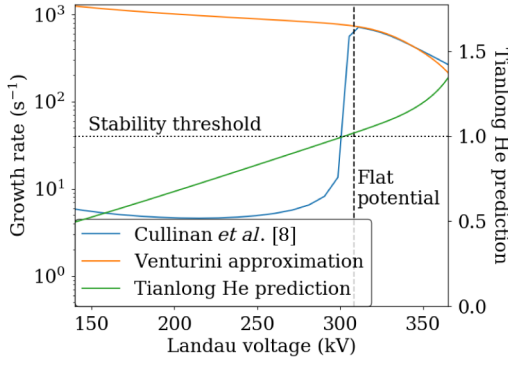
FIG. 1. Predictions for the stability of mode +1 for different Landau voltages using three different theoretical approximations [3,8,10]. The stability threshold is the radiation damping rate on the left axis and 1.0 on the right axis.

A mode-1 instability has been observed in the 3 GeV storage ring at MAX IV, a fourth-generation synchrotron light source that makes use of passive Landau cavities. In fact, both modes +1 and −1 have been observed and these are excited by a combination of the fundamental modes of the Landau cavities with the fundamental mode of a parked main cavity that was detuned significantly below the rf frequency. The presence of the parked main cavity does influence the instability thresholds and the mode number but the Physics is largely the same, as will be demonstrated. The phrase "mode-1 instability" is therefore used here to refer to both modes.

II. THEORETICAL BACKGROUND

Figure 1 shows predictions of whether mode +1 is stable or not for the parameters of the MAX IV 3 GeV ring [7] given in Table I running at a beam current of 200 mA, with a uniform fill (all rf buckets filled with the same bunch

TABLE I. Parameters of the MAX IV 3 GeV ring without insertion devices and the cavity parameters including the shunt impedance R_s per cavity along with its definition where V and P are the voltage and power in the cavity, respectively.

Parameter	Value
Energy E_0	3 GeV
Circumference	528 m
rf frequency f_{rf}	99.931 MHz
Harmonic number h	176
Energy loss per turn U_0	363.8 keV
Radiation damping time $\mathcal{T}_0$	25.194 ms
Momentum compaction α_c	0.000306
Natural normalized energy spread	0.000769
Landau cavity (LC) harmonic	3
LC shunt impedance $R_s = V^2/(2P)$	2.75 MΩ
LC quality factor	20,800
MC loaded shunt impedance	0.320 MΩ
MC loaded quality factor	3688

charge), with three Landau cavities and a main-rf voltage of 1 MV from 5 active main cavities (none parked). Predictions of three different theories are shown: one by three of the current authors [8] based on the approach taken by Thompson and Ruth [9], an approximation by Venturini within a more comprehensive analysis [Eq. (47) in [3]] and a stability prediction based on the method of Tianlong He [10]. This last method does not predict a growth rate but rather calculates the amplification of a mode +1 perturbation: it returns a value that is greater than one if mode +1 is predicted to be unstable and less than one otherwise. It should be noted that the approximation of Venturini is only valid for a limit of very low incoherent synchrotron frequency, which is why it matches well with the theory of the current authors in the regime close to flat-potential conditions and for overstretched bunches. The switch to this regime is very clear in the theory of the current authors and is predicted to occur very close to the flat-potential condition. The reason for this is the lowering of the incoherent synchrotron tune to close to zero. This also lines up with the unity crossing in the prediction from Tianlong He, which is not surprising because the physics and the main assumptions behind the two approaches are the same. Although the latter does not predict growth rates, it is simpler because, by focusing solely on mode +1, it bypasses the need to calculate a whole matrix.

In light of these predictions, the nature of the mode-1 instability can be understood to some extent. From inspection of Eq. (17) in [8], the condition for a large growth rate which dominates the radiation damping is

$$\frac{\text{Im}(\lambda)}{2\text{Re}(\Omega)} \gg \frac{1}{\mathcal{T}_0}, \tag{1}$$

where λ is an eigenvalue of the coupling matrix defined in Eq. (14) in [8], Ω is the complex coherent frequency and $\mathcal{T}_0$ is the radiation damping time. It can be seen that an instability with a low coherent frequency of oscillation $\text{Re}(\Omega)$ is likely to fulfill this condition.

The expression for $\text{Re}(\Omega)$ is given by Eq. (16) in [8]:

$$\text{Re}(\Omega)^2$$
$$= \frac{\text{Re}(\lambda) - 1/\mathcal{T}_0^2 + \sqrt{(\text{Re}(\lambda) - 1/\mathcal{T}_0^2)^2 + \text{Im}(\lambda)^2}}{2}. \tag{2}$$

Substituting this into the square of Eq. (1) and multiplying both sides by $\mathcal{T}_0^2$ gives

$$\frac{2(\frac{\text{Im}(\lambda)\mathcal{T}_0}{2})^2}{\text{Re}(\lambda) - \frac{1}{\mathcal{T}_0^2} + \sqrt{(\text{Re}(\lambda) - \frac{1}{\mathcal{T}_0^2})^2 + \text{Im}(\lambda)^2}} \gg 1. \tag{3}$$

The denominator on the left-hand side is small under the following conditions

$$\left(\frac{\text{Im}(\lambda)}{\text{Re}(\lambda) - \frac{1}{T_0^2}}\right)^2 \ll 1, \qquad \text{Re}(\lambda) < 0. \qquad (4)$$

After conversion of the wake function to impedance (see Appendix B), inspection of the coupling matrix in [8] reveals what this means in terms of the reactive impedance $\text{Im}(Z)$:

$$-q_b|F|^2\{\omega_{1-}\text{Im}[Z(\omega_{1-})] + \omega_{1+}\text{Im}[Z(\omega_{1+})]\}$$
$$\gg \frac{E_0 T_0^2}{e_0 \alpha_c}\omega_s^2, \qquad (5)$$

where q_b is the magnitude of the bunch charge, ω_s is the incoherent angular synchrotron frequency, T_0 is the revolution time, α_c is the momentum compaction factor, E_0 is the beam energy, e_0 is the elementary charge, F is the bunch form factor at the operational rf harmonic of the Landau cavities n and $\omega_{1\pm} = n\omega_{\text{rf}} \pm 2\pi/T_0 \pm \text{Re}(\Omega)$ are the nearby angular coherent synchrotron sidebands of the mode-$(+1)$ instability. Bunch-lengthening Landau cavities with excess shunt impedance have a large negative reactive impedance at ω_{1+}, significantly larger in magnitude than at ω_{1-} where it is positive (see Fig. 12 in Sec. IV). Furthermore, the incoherent angular synchrotron frequency ω_s is significantly reduced. Both of these factors contribute to fulfill the condition given by Eq. (5). A large real part of the impedance will also contribute but is not the dominant factor, as remarked by Venturini [3].

So far, the discussion has neglected Landau damping, which is present thanks to the spread in synchrotron frequency within each bunch due to the anharmonicity introduced to the total rf potential by the Landau cavities. This is expected to be particularly significant when close to flat-potential conditions. On the other hand, an instability with a very low coherent oscillation frequency may be expected to be resistant to such Landau damping due to its frequency being outside of the distribution of frequencies within the bunch.

In order to account for Landau damping, we use the Krinsky dispersion relation [11] for a quartic potential, as formulated by Lindberg [Eq. (50) in [12]]:

$$1 = \frac{\lambda_0 \sigma_\tau}{\alpha_c \sigma_\delta}\frac{128\pi e^{-\pi}}{\Gamma(1/4)(1 + e^{-\pi})^2}\int_0^\infty \frac{x^{5/2}e^{-x^2}}{\xi^2 - x}dx. \qquad (6)$$

Here, λ_0 is the eigenvalue of the coupling matrix defined in Eq. (19) in [12] (which is similar but not equivalent to the aforementioned coupling matrix for λ), σ_τ is the rms bunch duration, σ_δ is the normalized relative energy spread, $\Gamma(x)$ is the Gamma function and ξ is a normalized coherent frequency defined as

$$\xi = \frac{\Gamma(1/4)}{2^{5/4}\Gamma(3/4)^2}\frac{\Omega\sigma_\tau}{\alpha_c\sigma_\delta}, \qquad (7)$$

where Ω is the complex coherent frequency. What is important is that stability is determined by whether the value of λ_0 sits within or outside of Landau contours in complex frequency space as this corresponds to whether the beam is predicted to be stable or unstable, respectively. Finding the beam current at which the contour is crossed is therefore a method of determining the threshold current for a coupled-bunch instability. An example of such a calculation is shown in Fig. 2.

Under certain assumptions, specifically a particular incoherent synchrotron frequency, no Landau damping and a small difference between the coherent and incoherent synchrotron frequencies, the eigenvalue λ_0 can be interpreted as a complex frequency shift, where the imaginary component is the growth rate. This may be useful for comparing the stability of a higher-order-mode-driven (HOM-driven) coupled-bunch mode with and without Landau cavities but since the fundamental modes of the Landau cavities are expected to be the source of the instability in this case, the utility here is not so obvious.

Another limitation of Eq. (6) is that it assumes a perfect quartic potential. For a passive Landau cavity system and fixed rf voltage (and all other relevant machine parameters constant), this can only be true at one beam current. Nevertheless, as can be seen in the following sections, this method has been used to predict trends in the threshold current with some success, even for conditions where the flat potential obtained is clearly very different from a quartic potential.

Because they neglect the Landau damping, the approximations shown in Fig. 1 tend to predict a mode-1 instability at flat potential when one is not seen in reality. The Krinsky dispersion relation was found to be more successful when comparing with measurements and so is used for all theoretical predictions presented in Sec. III unless otherwise stated. Although the complete analysis of
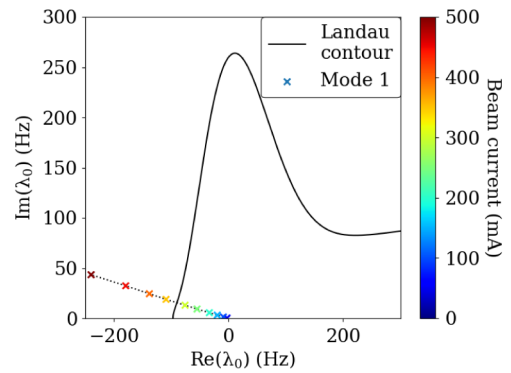
FIG. 2.　Stability diagram, as predicted by the theory presented in [11], for a beam in a quartic potential with an rf voltage of 1 MV and the impedance given by the fundamental of the harmonic cavities. If the parameter λ_0 is within the Landau contour, it is predicted to be stable due to Landau and radiation damping.

Venturini [3] does also include Landau damping, and for arbitrary rf potentials, it is numerically more complex to solve. Macroparticle tracking includes Landau damping as well but requires significantly more computing resources. The simulations must include selective damping of the Robinson instability and enough macroparticles to accurately model the Landau damping (further increasing the computing resources). This is therefore also left for further work. The active main-rf cavities are always included in the theoretical predictions but their influence is negligible.

III. EXPERIMENT

The mode 1 instability has been observed at the 3 GeV ring at MAX IV for quite some time [13]. Initially, attempts to understand it focused on the possibility that it was a mode-coupling instability similar to the observed mode-0 instability (see Appendix C). Recently, a concerted effort has been made to reproduce the instability reliably enough to study it systematically. The latest measurements have been made using the streak-camera setup installed in late 2021 [14]. The streak camera was set up in dual-time-base mode: a synchroscan unit streaking vertically at the rf frequency (one forward sweep every rf period synchronized with the electron bunch) and a second slower streak along the horizontal axis covering 5 μs, which corresponds to just under three revolution periods. Although the limited horizontal resolution means that individual bunches cannot be distinguished, this setup allows for single-shot measurements of the evolution of the bunch profile over the bunch train. Sequences were taken of one hundred single-shot measurements with an interval of 120 ms between them. This is slightly below the 10 Hz maximum acquisition rate of the setup to ensure equally spaced images. Assuming the mode number is known, this acquisition rate limits measurements of the coherent oscillation frequency of the instability to a maximum of 8.3 Hz while the total acquisition time for the 100 shots defines the frequency resolution of 0.08 Hz.

Figure 3, shows three frames of a mode-(−1) instability. It has the distinct appearance that led to it sometimes being referred to as "periodic transient beam loading" [4] and is clearly oscillating (clear shift in phase between images). The shift in phase over a given time period is an illustration of the coherent frequency.

In order to observe the instability shown in Fig. 3, the fill pattern must be sufficiently uniform. This is because, when the Landau cavities are tuned such that the total rf voltage is close to flat, inhomogeneous beam loading of the cavities due to small differences in charge between bunches can lead to large differences in their profiles.

Accumulation in the MAX IV 3 GeV ring is achieved by injecting trains of around ten ring bunches from the full-energy linac injector [15] and stepping the timing of the linac between shots to change the target bucket number. The linac pulse does not have a square current profile so the
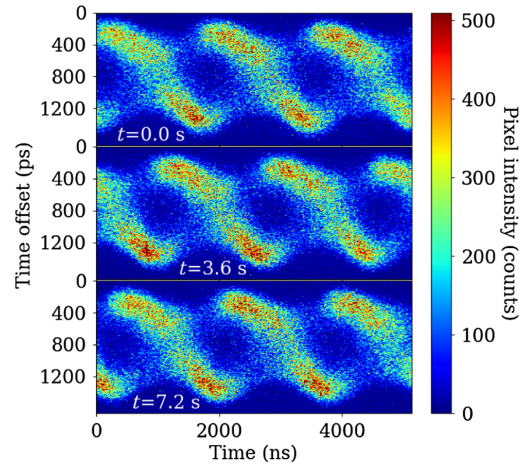
FIG. 3. A mode-(−1) instability as seen in three streak-camera images equally separated in time over a period of 7.2 s with a beam current of 240 mA, an rf voltage of 1 MV and a Landau voltage of 337 kV.

step size is deliberately not a factor of the harmonic number. This ensures that, provided enough linac pulses are used during an injection, all ring rf buckets receive charge from all parts of the linac pulse and therefore, roughly equal total charge. In order to increase the fill-pattern uniformity even further during these tests, the charge in each linac pulse was reduced to increase the total number of pulses required to fill the machine to high current. The measurements were then performed on a decaying beam.

Figure 4 demonstrates why this is important. Under the conditions of the measurement, with a uniform fill, stable overstretched bunches are obtained with a Landau voltage of 376 kV. With a slightly nonuniform fill, on the other
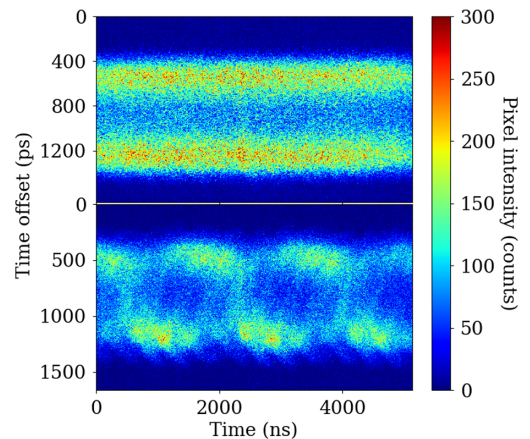
FIG. 4. Single-shot dual-timebase streak-camera measurement at 300 mA of beam current for a uniform fill and Landau voltage of 376 kV (top) and a nonuniform fill and Landau voltage of 372 kV (bottom) with a main-rf voltage of 1.13 MV. The horizontal time axis covers just under three machine revolution periods. Both images remain stable from frame to frame.

hand, already at a Landau voltage of 372 kV, inhomogeneous beam loading leads to significant variation in the longitudinal charge profiles of the different bunches. This variation is very similar to a single frame of the mode-(-1) instability in Fig. 3 but does not oscillate: the picture remains stable from frame to frame. A Landau voltage of 376 kV could then not be reached without a mode-1 instability developing. The fill-pattern uniformity clearly has a large impact on the dynamics and nonuniformity can make accurate measurement of the thresholds impossible. It is therefore essential that, for a mode-1 instability to be identified, it must be oscillating and to obtain consistent results, it must develop from a uniform fill. Once excited, any modulation of the coherent frequency of the instability is an indication that there is still some nonuniformity present.

Figure 5 shows the fill patterns measured using time-correlated single-photon counting [16] at the times when the two images in Fig. 4 were taken. In this case, an increase in the normalized standard deviation in the bunch charges from 0.5% to 1.7% (and the time structure of this increased charge variation) was enough to cause the change from uniformly overstretched bunches to large variation in the bunch profiles. The precise fill-pattern diagnostic used for this measurement was acquired after the bulk of the results presented in this paper were obtained. Nevertheless, the importance of this effect was already understood and so the fill-pattern was always kept as uniform as possible using the precautions mentioned above.

Something that proved crucial in these experiments was the mode-0 damper [17]. This is because modes ± 1 were both seen exclusively in conditions where mode 0 would otherwise be unstable due to a mode-coupling instability [13]. The measurements took place over a period of two years during which three cavities (one Landau and two main) were removed from the ring for unrelated reasons. The combination of cavities present in the ring is specified explicitly in each subsection. Table II provides a summary for reference.
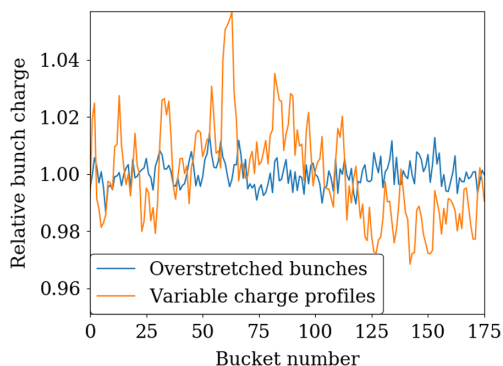
TABLE II. Combination of main and Landau cavities present in the MAX IV 3 GeV ring during the measurements for each subsection where results are presented.

Section	Number of active MCs	Number of LCs	Parked MC
III A	5	3	Yes
III B	4	2	Yes
III C	4	2	No
Appendix B	4	2	Yes

A. Instability thresholds

In order to measure instability thresholds for the mode-1 instability, first the ring was injected in a uniform fill pattern up to a current of 300 mA with an rf voltage of 1 MV. The Landau cavities were then tuned toward resonance, increasing the cavity voltage and if present, the mode-1 instability was measured using the streak camera. The presence of the mode-1 instability reduces the measured Landau voltage and so the autotuning would often react, tuning the cavities even closer to resonance to maintain the set cavity voltage. This was compensated for by reducing the set voltage when necessary. The process was then repeated at a different beam current. To move on to the next current step, the Landau cavities were detuned once more and a beam scraper was inserted in order to lower the beam lifetime until the current had reached the desired lower value. The reason for detuning the Landau cavities first is the presence of the mode-1 instability could introduce a nonuniformity in the fill pattern when scraping down the beam current. These measurements were made with three Landau cavities installed in the ring (total shunt impedance 8.25 MΩ as per Table I), five main-rf cavities active and one parked.

Figure 6 shows the results. No mode-1 instability was observed in the empty regions of the plots. The saturation amplitudes and coherent frequencies were extracted from the streak camera images as follows. First, for each image, the centre of charge in time offset $\langle \tau \rangle_m$ was taken from an intensity-weighted average of the pixel time coordinates along the vertical axis for each column m of pixels:

$$\langle \tau \rangle_m = \frac{\sum_{n=0}^{N-1} \tau_n P_n}{\sum_{n=0}^{N-1} P_n}, \tag{8}$$

where τ_n is the time coordinate of pixel n along the vertical axis, P_n is the intensity measured by said pixel and N is the number of pixels in each column. The amplitude A_1 and phase θ_1 of mode ± 1 in each image was then calculated from a Fourier transform of the centres of charge along the horizontal axis knowing the wave number of mode ± 1: $2\pi/T_0$.

FIG. 5. Fill patterns corresponding to the two images in Fig. 4 as measured using time-correlated single-photon counting.
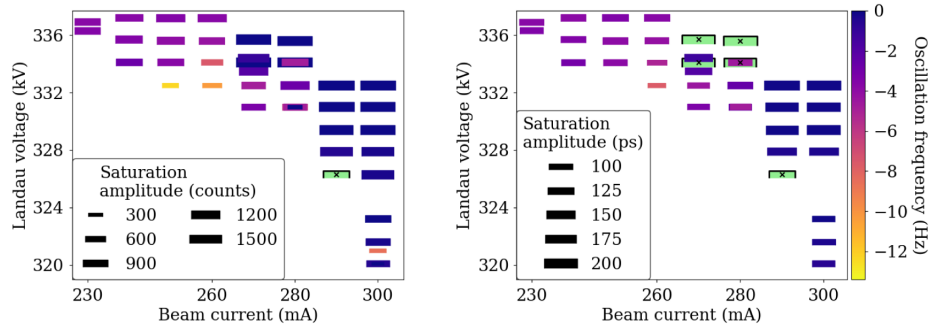
FIG. 6.   Amplitudes and coherent frequency of a mode-1 instability with 6 MCs (5 active, 1 parked) and 3 LCs as measured using bunch-by-bunch phase-detection (left) and sequences of streak-camera images (right) with an rf voltage of 1 MV. Negative oscillation frequencies correspond to mode −1 while light green patches outlined on three sides and with a cross over the top indicate a positive oscillation frequency (mode +1).

$$A_1 e^{i\theta_1} = \frac{1}{M} \sum_{m=0}^{M-1} \exp\left(i2\pi \frac{t_m}{T_0}\right) \langle \tau_m \rangle_m, \qquad (9)$$

where t_m is the time coordinate of pixel column m and M is the total number of columns. The saturation amplitude was then determined from the mean value of A_1 over all the images in a sequence and the coherent frequency was taken from a linear fit of the θ_1 values over time given the known time separation of the images.

Data was also taken using the bunch-by-bunch (BBB) phase-detection capabilities of a Dimtel feedback system [18] and the saturation amplitudes and coherent oscillation frequencies were extracted by Fourier transform in a similar way. This data allowed for measurement of the coherent frequencies to larger values since the sampling rate is a lot faster. In fact, the turn-by-turn sampling rate had to be limited to once every 32 turns in order to maximize the acquisition time to around 4 s and maximize the frequency resolution. This is still shorter than the total acquisition time of the one hundred streak-camera shots (12 s) so the streak camera still has better frequency resolution. Another advantage of the streak camera is that it provides calibrated time axes while the scale of the bunch-by-bunch phase detection is not calibrated by default and calibration is unreliable for the large phase-excursions seen. This is why the saturation amplitudes in Fig. 6 are displayed in counts and only relative differences can be compared with the calibrated amplitudes measured using the streak camera.

There is good agreement between the two measurement methods, although the streak camera occasionally underestimates the oscillation frequencies due to its limited bandwidth and aliasing. As predicted, the measured coherent frequency, with a maximum magnitude of just over 12 Hz, is always low compared to the average incoherent synchrotron frequency of around 130 Hz in a quartic potential. For a harmonic oscillator, a lower frequency of oscillation means there is a weaker restoring force and therefore a lower amount of energy stored in the system for

a given peak excursion and so the appearance of a mode-1 instability does not lead to a large increase in the energy spread.

The frequency axis in Fig. 6 is such that a negative oscillation frequency corresponds to mode −1. Positive frequencies are colored light green and are generally very low in magnitude, less than 1/3 Hz and mostly too small for the BBB measurement to resolve. The results indicate that mode −1 was observed much more frequently than mode +1. This is because of the presence of the parked main cavity as discussed in detail in Sec. III B and Sec. IV.

The results shown in Fig. 6 are for conditions that would lead to overstretched bunches if the beam were stable. An attempt was also made to establish the thresholds for the mode-1 instability that would prevent the flat-potential condition from being reached. For each beam current, the rf voltage was reduced until the Landau voltage corresponding to flat potential, as calculated using the theory presented in Appendix A, could not be reached without the mode-1 instability appearing (specifically in this case mode −1). Similar to before, the Landau voltage also had to be reduced between each step to ensure that the appearance of the mode-1 instability was not a transient effect caused during the reduction in the rf voltage. These mode-1 instability thresholds are shown in Fig. 7. Example outcomes of Landau-voltage and bunch-length calculations are listed in Table III (see columns labeled "3LCs").

There is some numerical noise in the determination of exactly when the Landau contour is crossed but the trend in the theoretical predictions is clear and so a linear fit could be performed. The rf voltages for which mode −1 appears are all lower than those that have typically been used during user operation of the MAX IV 3 GeV ring. However, continuing the measured trend predicts that an rf voltage of 1.48 MV would be needed for a threshold current of 500 mA (the design current). This would place significant demands on the power required from the rf transmitters.

The theoretical predictions do not account for the presence of the parked main cavity. Unfortunately, the
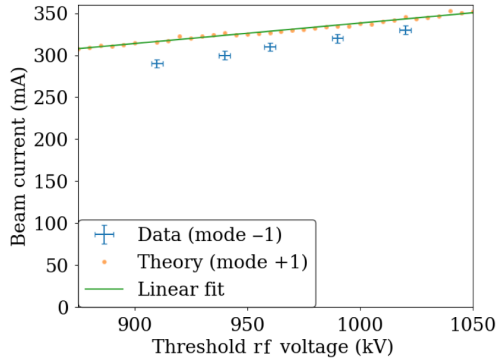
FIG. 7.   Threshold currents of the mode-1 instability for different rf voltages as measured (mode -1) in the MAX IV 3 GeV ring with 6 MCs (5 active, 1 parked) and 3 LCs and as predicted (for mode $+1$) using the Krinsky dispersion relation, Eq. (6) in Sec. II. The errorbars correspond to half the step sizes in the scans of current and rf voltage.

importance of this was not realized until after the cavity in question had actually been removed from the ring for the testing and installation of HOM dampers. This prevented any measurement of its exact resonant frequency so that it could be included in the theoretical predictions. Just before the removal, one passive Landau cavity was also removed, and this prevents any attempt at reproducing these results without the parked cavity present.

The difference between the experimental results and the theoretical predictions in Fig. 7 is quite significant. Nevertheless, it is encouraging that they both show the linear relationship that has previously been found in simulation [4]. Tests of inserting a parked main cavity into the theoretical calculations with an arbitrary detuning changed the threshold currents but not the slope of the trend. The difference in the slope may be due to the presence of short-range wakefields, which are not included in the theory. The theory also assumes a longitudinally stable beam as a starting point while in reality, HOM-driven coupled-bunch modes were always present, albeit at low amplitude. The differences in the absolute values of the threshold currents cannot be commented on at this stage

because of the unknown impedance of the parked main cavity as previously mentioned.

Experimental investigations into the effect of a parked main cavity were made with the two Landau cavities and five main cavities remaining in the ring as outlined in the next section.

B. Parked main cavity

It had been known for some time that the removal of a Landau cavity could assist in the increase in the highest current at which a stable beam can be stored in the MAX IV 3 GeV ring both due to the mode-1 instability and the rf voltage required to achieve quartic potential. The disadvantage of the lower shunt impedance would be the inability to achieve flat potential at low currents. The decision to remove a Landau cavity was forced toward the end of 2022 by the discovery of a vacuum leak in one of them and this one was therefore removed from the ring in December of 2022. This provided an opportunity to test the influence of the total R/Q of the Landau cavities. First however, the impact of a parked main cavity, was investigated. As it is a normal conducting cavity with the input power coupler still attached, it is assumed that it is only the resonant frequency of the fundamental mode that changes when the cavity is parked and the shunt impedance and quality factor remain those given in Table I.

Measurements were made with the five main-rf cavities that remained in the ring. Four of the cavities were active and one was parked. First, the potentiometer readback from the tuning mechanism of the parked cavity was calibrated using drive-damp measurements [19] performed with the aforementioned bunch-by-bunch feedback system [18]. These measurements were made with an rf voltage of 1.13 MV, 20 mA of beam current in a uniform fill pattern and one insertion device closed for additional damping. The results are shown in Fig. 8. A Lorentzian fit was applied and the resulting bandwidth was used to determine a linear conversion from the reading of the potentiometer readback of the tuning mechanism to the detuning of the cavity, assuming the theoretical MC quality factor of 3688. An independent calibration was also made offline using a

TABLE III.   Outcomes of example calculations of Landau voltages for flat-potential conditions for different main-rf voltages. Threshold currents extrapolated or interpolated from the measured results are also given, although the voltages and bunch lengths are practically constant across the full current range.

rf voltage (kV)	Natural bunch length (ps)	Mode-1 threshold current (mA)		Landau voltage (kV)		Bunch length (ps)		Minimum current for flat potential (mA)	
		3 LCs	2 LCs	3 LCs	2 LCs	3 LCs	2 LCs	3 LCs	2 LCs
900	43.0	274	344	272	271	210	207	28.7	42.7
950	41.7	292	360	290	290	207	203	30.7	46.0
1000	40.4	310	377	308	308	203	199	32.6	48.8
1050	39.3	329	393	326	326	199	196	34.9	52.1
1100	38.3	347	410	344	343	195	194	36.9	54.9
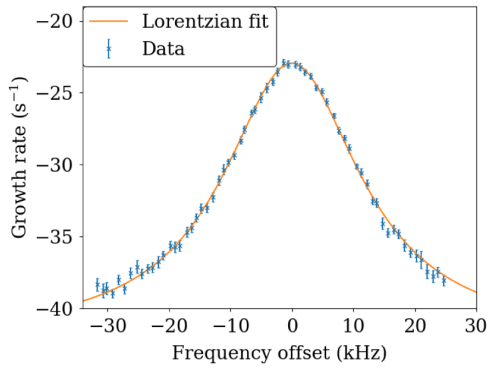
FIG. 8. Drive-damp measurements of the growth time of coupled-bunch mode -1 for different detunings of a parked main cavity from $f_{rf} - f_0$. The error bars are estimated from the uncertainty of the fits to the mode amplitudes and assuming a Gaussian response for the Chebyshev filter used in the signal processing.

FIG. 9. Measurements of the threshold current for different detunings of a parked main cavity from $f_{rf} - f_0$ compared to theoretical predictions using the Krinsky dispersion relation, Eq. (6) in Sec. II. The point-to-point variation between the data points is an indication of the statistical uncertainty.

network analyzer and the conversion gradient obtained was within 4% of the result obtained from the Lorentzian fit. The agreement in the intercept parameter was not as good, differing by the equivalent of 22 kHz on resonance, most probably due to a mismatch between the calibration of the network analyser and the assumed frequency of the machine main oscillator. The advantage of a beam-based calibration is that the exact same rf frequency that is used in the machine is essentially used as a reference signal in the measurements.

The peak growth rate measured from the Lorentzian fit is $+18.1 \text{ s}^{-1}$, which agrees to a similar level with the theoretical growth rate of $+19.2 \text{ s}^{-1}$. It is also reassuring that the growth rate without Landau-cavity bunch lengthening has the expected dependence on the frequency offset.

Mode -1 instability threshold currents were then measured for different parking frequencies of the inactive main cavity. For a number of different current levels, the parked cavity was tuned toward the resonant frequency of coupled-bunch mode -1 until it went unstable, at which point the frequency offset was recorded. At each beam current, the Landau voltage was set to the value corresponding to flat potential, as determined using the theory presented in Appendix A. This was done with the maximum obtainable rf voltage of 1.13 MV so that the mode-0 damper had enough gain to keep mode 0 stable across the whole current range. At the lowest beam currents at which measurements were taken, the Landau cavities had to be tuned close to resonance to reach flat potential conditions and so mode 0 was particularly unstable. This is the reason why results could not be obtained at lower beam currents.

The results are shown in Fig. 9. Unlike the dependence of the growth rate on the frequency offset without bunch lengthening shown in Fig 8, the dependence of the threshold current with bunch lengthening is very asymmetric and the threshold currents are lower for negative frequency offsets.
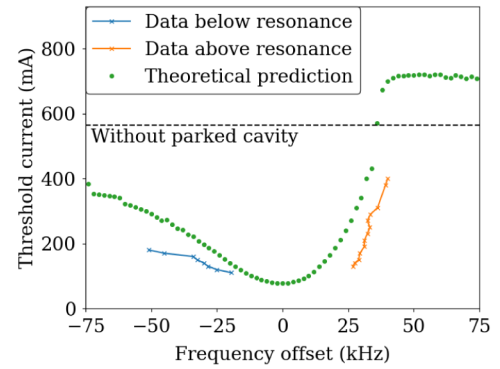
This is seen very clearly in both the theoretical predictions and the experimental results and is due to the influence of the parked cavity on the coherent frequency of the instability, as discussed below in Sec. IV. Overall, the theory tends to overestimate the threshold currents quite significantly but once again, follows the trend seen in the experimental results very well. As mentioned in the previous section, the reason for the discrepancy could be the presence of low-amplitude HOM-driven coupled-bunch instabilities and the short-range wakefields, neither of which are included in the theory and which could negatively impact both the bunch lengthening and the Landau damping.

C. Two Landau cavities

Measurements of the mode-1 instability with two Landau cavities were made in the autumn of 2023. By this time, an additional main-rf cavity had been removed from the ring, also for the installation of HOM dampers. Measurements were therefore made with four main cavities active and none parked. The measurements performed were otherwise very similar to those presented in Sec. III A. Although the results cannot be directly compared due to the unknown influence of the parked main cavity in Sec. III A, they show the expected difference from the reduction in the Landau-cavity R/Q and also confirm that it is mode $+1$ that is excited by the Landau cavities.

Figure 10 shows the amplitude and coherent frequency of the instability for different beam currents and Landau voltages at a total rf voltage of 1.13 MV. The reason that a higher rf voltage was used than in Sec. III A was so that mode-0 was kept stable at high current over a broad range of Landau voltages. Once again, there is good agreement on the coherent frequencies between the results using the BBB phase detection and the streak camera. The only points at which they differ are when the coherent frequency is too high for the streak-camera sampling rate, which leads to aliasing. Although the BBB does not provide calibrated values for the
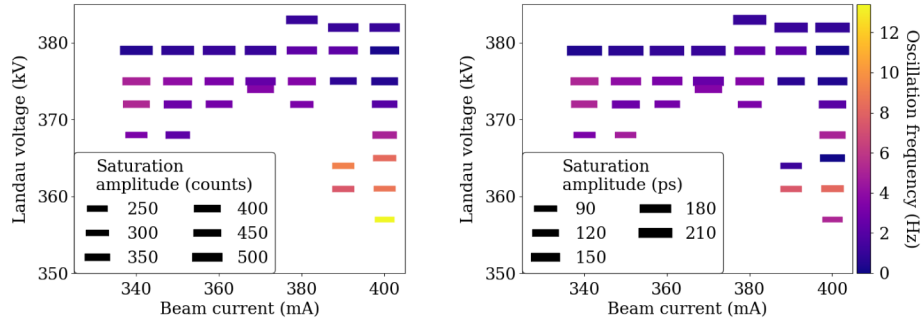
FIG. 10.   Amplitudes and coherent frequency of a mode-1 instability with 4 active MCs and 2 LCs as measured using bunch-by-bunch phase-detection (left) and sequences of streak-camera images (right) with an rf voltage of 1.13 MV.

oscillation amplitudes, the relative amplitudes of the different points agree between the two methods.

Unlike the coherent frequencies shown in Fig. 6, all of those shown in Fig. 10 are positive confirming that without the presence of the parked main cavity, it is mode +1 that is driven by the Landau cavities. Something that was not observed with three Landau cavities but that was observed here was that when steadily increasing the Landau voltage, there came a point at which the mode-1 instability disappeared and stable overstretched bunches formed. This occurred for Landau voltages above around 383 kV and at beam currents of 370 mA and lower.

Figure 11 is the analog of Fig. 7 for two Landau cavities and no parked main cavity. Example cavity voltages in this case are given in columns labeled "2 LCs" in Table III. The theory overestimates the measured threshold currents to a very similar level to in Fig. 9. However, once again, the measured trend is very similar to the predicted one and shows a linear dependence on the rf voltage for the threshold current of the mode-1 instability at flat potential. Unlike in Fig. 7, the slopes of the measured and predicted trends are here very similar, differing by less than 10%. Also included in the figure are predictions using the method

of Tianlong He [10]. The theory of the current authors [8] is not included in the figure but predicts something very similar as expected. As anticipated, these methods significantly underestimate the threshold currents because they do not include the Landau damping.

In general, the threshold current at a given rf voltage is significantly higher with two Landau cavities than with three due to the R/Q being lower by a third.

As well as threshold currents, the Krinsky dispersion relation [11] can be used to make predictions of the coherent frequencies. These predictions were around 50 Hz for all rf voltages. The measured coherent frequencies, on the other hand, were in the order of 1 Hz. However, the prediction applies to an instability growing from a stable beam whereas all of the coherent frequencies were measured on the instability in saturation.

IV. CAVITY IMPEDANCES

Looking at the cavity impedances in the relevant frequency range can help to form a qualitative understanding of the experimental results and in particular, why mode −1 was observed instead of mode +1 when a parked main cavity was present. Figure 12 shows the reactive impedance of five active main cavities, three Landau

FIG. 11.   Threshold currents of the mode-1 instability for different rf voltages as measured in the MAX IV 3 GeV ring with 4 active MCs and 2 LCs and as predicted using the Krinsky dispersion relation and the Tianlong He method, both discussed in Sec. II. The errorbars correspond to half the step size in the scan of rf voltage.
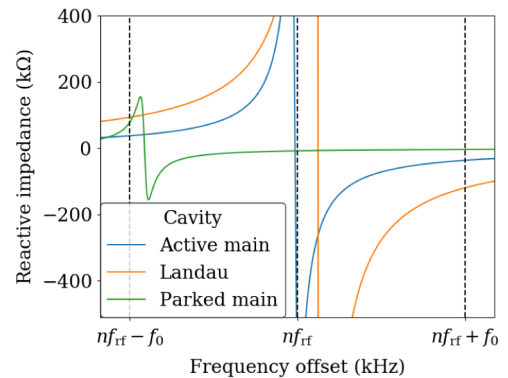
FIG. 12.   Reactive part of the impedance for flat-potential conditions with a beam current of 200 mA, three Landau cavities and an rf voltage of 1 MV. For the Landau impedance $n = 3$ while for the main cavities $n = 1$.
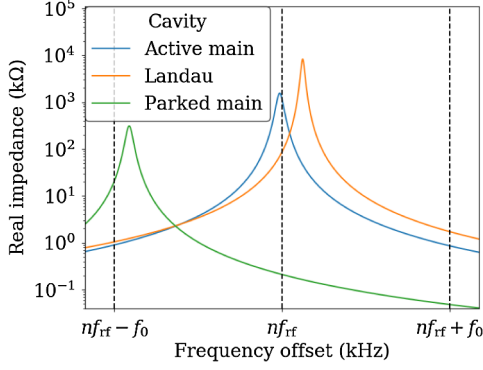
FIG. 13. Real part of the impedance for flat potential conditions with a beam current of 200 mA, three Landau cavities and an rf voltage of 1 MV. For the Landau impedance $n = 3$ while for the main cavities $n = 1$.

cavities and a single parked main cavity for flat potential conditions and a beam current of 200 mA and a main rf voltage of 1 MV. To first order, the reactive impedance is the dominant factor in determining the coherent frequency of the instability and the relevant frequencies for coupled-bunch modes ± 1 are the synchrotron sidebands of the revolution harmonics $nf_{rf} \pm f_0$ marked in the figure, where $n = 1$ for the active and parked main cavities while $n = 3$ for the Landau cavities. The reactive impedance affects both modes similarly and it is clear that the reactive impedance of the Landau cavities is dominant.

When it comes to determining which mode is unstable and which one is damped, the real part of the impedance is more important. This is shown in Fig. 13. Generally speaking, a larger impedance at the $nf_{rf} + f_0$ harmonics than at the $nf_{rf} - f_0$ harmonics means that the coupled-bunch mode $+1$ is more likely to be unstable, and vice versa for coupled-bunch mode -1. Here, it is clear that the parked main cavity is the dominant source of real impedance and is driving mode -1 and damping mode $+1$. This is a simplified explanation and neglects effects such as Landau damping and the interplay between the coherent frequency and the growth rate.

The parked main cavity can have a significant impact on the threshold current, as shown in Sec. III B, but its reactive impedance will only be dominant very close to resonance. Here, when tuned below $f_{rf} - f_0$, it will combine with the Landau cavities and further lower the coherent frequencies of modes ± 1 while when tuned above, it will push the coherent frequencies to higher values. Depending on the tuning of the parked main cavity, the difference between the stability of the two modes may not be large, as evidenced by the fact that both feature in Fig. 6, although predominantly mode -1.

V. CONCLUSION

The mode-1 instability has been observed and investigated in the 3 GeV ring at MAX IV. The expected

dependence on the rf voltage was observed. It was also found that prediction methods that neglect the Landau damping may significantly underestimate thresholds of the mode-1 instability.

The removal of a Landau cavity from the ring provided an opportunity to see how a reduction in the R/Q relaxed the thresholds of the instability. As it significantly impacted the results, the effect of a parked main cavity was also investigated. The measured threshold currents showed an asymmetric dependence on the detuning of the parked cavity around the frequency of coupled-bunch mode -1 and that the presence of a parked cavity can both decrease and increase the threshold of a mode-1 instability.

The mode-1 instability does not at present limit the bunch lengthening that can be achieved in the 3 GeV ring at MAX IV. The rf voltage of 1.13 MV that is currently used during operation of is large enough that the threshold current of the mode-1 instability at flat potential is above the operating current of 400 mA. It is therefore not necessary to switch to an uneven filling pattern, which would degrade the bunch lengthening [8].

Many new fourth-generation light-source storage rings are expected to come online during the next decade and the use of Landau cavities is an essential component of their design [20]. It is therefore very important that the mode-1 instability be avoided and for that, accurate threshold predictions must be made. This investigation provides useful information to those making these predictions. With this in mind, all of the experimental results displayed here have been uploaded as Supplemental Material [21] and the computer code used to evaluate the theoretical predictions has been uploaded to Github [22].

APPENDIX A: DETERMINATION OF FLAT POTENTIAL CONDITIONS IN A PASSIVE SYSTEM

The following gives a procedure for determining the Landau voltage and phase to cancel out the first derivative of the main rf and deliver flat-potential conditions. Following the convention in [1], the voltage and its first derivative are written

$$V_T(\varphi) = V_{rf}[\sin(\varphi + \phi_s) + k\sin(n\varphi + n\phi_h)], \quad \text{(A1)}$$

$$V'_T(\varphi) = V_{rf}[\cos(\varphi + \phi_s) + kn\cos(n\varphi + n\phi_h)], \quad \text{(A2)}$$

where φ is the phase, n is the harmonic of the main rf at which the Landau-cavity system operates, V_{rf} is the main rf voltage and k is the voltage fraction (Landau voltage

divided by the main-rf voltage). The synchronous phases ϕ_s and $n\phi_h$ are such that $V_T(0) = U_0$ where eU_0 is the energy loss per turn due to synchrotron radiation and e is the elementary charge.

To obtain a flat potential, the derivative of the total rf voltage must be zero at the synchronous phases. If the synchronous phase of the main rf is eliminated, the following condition is obtained for $V_T'(0) = 0$:

$$[(1 - n^2)\sin^2(n\phi_h) + n^2]k^2 - 2\frac{U_0}{V_{\rm rf}}\sin(n\phi_h)k$$

$$+ \frac{U_0^2}{V_{\rm rf}^2} - 1 = 0. \tag{A3}$$

In the case of a fully-active system, this condition can be achieved for a continuum of Landau voltages and phases: as long as the voltage fraction k is large enough, there exists a phase where this condition can be met.

With passive Landau cavities on the other hand, there is only one solution for k and ϕ_h if all other parameters are fixed. From Eqs. (18) and (19) in [1], under the approximation of a scalar form factor,

$$\sin(n\phi_h) = -\frac{kV_{\rm rf}}{2IFR_s}, \tag{A4}$$

where I is the beam current, F is the scalar bunch form-factor at the Landau-cavity harmonic n and R_s is the total Landau-cavity shunt impedance. Substituting Eq. (A4) into Eq. (A3) gives the following expression

$$\frac{(1 - n^2)V_{\rm rf}^2}{(2IFR_s)^2}k^4 + \left(n^2 + \frac{U_0}{IFR_s}\right)k^2 + \frac{U_0^2}{V_{\rm rf}^2} - 1 = 0. \tag{A5}$$

This can be solved for k using the quadratic formula. Once k is obtained, Eq. (A4) can be used to determine the Landau-cavity field phase and from that, the tuning angle and cavity detuning. For most accurate results, the solution should be determined self-consistently, calculating the resulting bunch profile and iterating on the form factor as in [1]. The approximation of a scalar form factor is a shortcoming but in practice, the equations still deliver accurate results for a large range of parameters and have proved useful for operation of the 3 GeV ring at MAX IV.

At a particular beam current, the flat-potential conditions will correspond to a quartic potential and this beam current can be varied by changing the rf voltage $V_{\rm rf}$, making a quartic potential also accessible over a wide range of beam currents with a fully passive system and a fixed Landau-cavity shunt impedance. However, lower beam currents will require a lower rf voltage and this may compromise the beam lifetime.

Equation (A5) has no real roots when the beam current is too low to generate the required fields. The expression for the minimum current at which a flattened potential can be obtained is therefore given as

$$I_{\min} = \frac{-U_0 + \sqrt{(1 - n^2)(U_0^2 - V_{\rm rf}^2)}}{R_s F n^2}. \tag{A6}$$

This equation neglects the fact that it may be impossible to reach flat potential at low currents due to a Robinson instability.

APPENDIX B: TRANSFORMATION TO IMPEDANCE

We follow the approach of Ng [23]. Equation 11 for the coupling matrix $\mathbf{M}_{lj}$ in [8] reads

$$\mathbf{M}_{lj} = \sum_{n=0}^{\infty} \mathrm{Re}\{F_l^* F_j q_j W'[nT_0 + \Delta t_{lj}(\tau_l, \tau_j)]\}$$

$$\times \frac{r_j(nT_0)}{\hat{r}_j}, \tag{B1}$$

where W' is the derivative of the wake function, F_j is the form factor of bunch j at the operational rf harmonic of the Landau cavities and τ_j is its time offset and Δt_{lj} is the time difference between bunches l and j as defined in [8].[1] The limitation to a resonant wakefield in the use of a form factor is a little early here but makes sense in the context of the original publication and will eventually be justified here. The assumed motion of bunch j is $r_j(t) = \hat{r}_j \exp(i\Omega t)$ where Ω is the coherent frequency and $\hat{r}_j$ is its peak time offset.

To convert to impedance, the following definition is used

$$W'(t) = \frac{i}{2\pi} \int_{-\infty}^{\infty} e^{-i\omega t} \omega Z(\omega) d\omega, \tag{B2}$$

where ω is the angular frequency. Using the following identity:

$$\sum_{k=-\infty}^{\infty} e^{ikz} \equiv 2\pi \sum_{p=-\infty}^{\infty} \delta(z - 2\pi p), \tag{B3}$$

exploiting the causality of the wake function $W(t < 0) = 0$ and changing the variable of integration to $y = (\omega - \Omega)T_0$, Eq. (B1) becomes

$$\mathbf{M}_{lj} = \frac{i|F|^2 q_b}{T_0} \sum_{p=-\infty}^{\infty} \left(\frac{2\pi p}{T_0} + \Omega\right) Z\left(\frac{2\pi p}{T_0} + \Omega\right)$$

$$\times \exp\left[-i\left(\frac{2\pi p}{T_0}\right)\Delta t_{lj}(0, 0)\right], \tag{B4}$$

---

[1]The subscripts l and j have been added for both brevity and to be more accurate.

where it has been assumed that the bunches are evenly spaced so that $\Delta t_{lj}(\tau_l, \tau_j) = \Delta t_{lj}(0,0)$ and all have the same form factor F and bunch charge q_b as expected in a uniform fill. Under these conditions, it is also justified to isolate mode 1 by setting $p_{1\pm} = \pm nh + 1$. We then obtain

$$\mathbf{M}_{lj} = \frac{i|F|^2 q_b}{T_0}[-\omega_{1-}Z(-\omega_{1-}) + \omega_{1+}Z(\omega_{1+})]$$
$$\times \exp[-i2\pi\Delta t(0,0)/T_0], \tag{B5}$$

where we have defined $\omega_{1\pm} = \pm 2\pi p_{1\pm}/T_0 \pm \mathrm{Re}(\Omega)$ and recognized that $\exp[-i2\pi p_{1\pm}\Delta t(0,0)/T_0] = \exp[-i2\pi\Delta t(0,0)/T_0]$. The real part of the coupling matrix is then given by

$$\mathrm{Re}(\mathbf{M}_{lj}) = -\frac{|F|^2 q_b}{T_0}$$
$$\times \{\omega_{1-}\mathrm{Im}[Z(\omega_{1-})] + \omega_{1+}\mathrm{Im}[Z(\omega_{1+})]\}$$
$$\times \exp[-i2\pi\Delta t(0,0)/T_0], \tag{B6}$$

where we have additionally made use of the fact that $\mathrm{Im}[Z(\omega)]$ is an odd function. Substituting this into Eq. (14) of [8] is the basis for the inequality in Eq. (5) here in the case of the mode-$(+1)$ instability. One additional assumption in Eq. (B6) is that the form factor does not change in the frequency range of $\omega_{1-} \le \omega \le \omega_{1+}$. This is generally justified.

APPENDIX C: COHERENT FREQUENCY

Robinson-mode coupling can cause a strong instability even when the dipole and quadrupole Robinson modes are predicted to be stable in isolation. Although no mode coupling is predicted for mode 1, an experiment was performed to try and confirm this. A longitudinal kicker cavity was used to drive the beam over a broad frequency band around the synchrotron tune. The combined signal from the four buttons of a beam-position monitor (BPM) pick up was connected to a spectrum analyser. The coherent frequencies of the dipole and quadrupole Robinson modes were then determined from the difference in frequency between the peak at the fifth harmonic of the rf and its synchrotron sidebands. An image of such a measurement is shown in Fig. 14. The fifth harmonic was chosen for increased BPM sensitivity compared to the first. Similarly, the coherent frequencies of coupled-bunch modes ± 1 were determined from the synchrotron sidebands at the first revolution harmonic above the fifth rf harmonic. The measurements were made with two Landau cavities in the ring, four active main cavities and one parked. Unless explicitly mentioned, the parameters used are those listed in Table I.

The measurements were performed at 90 mA and with an rf voltage of 689 kV. This combination is predicted to
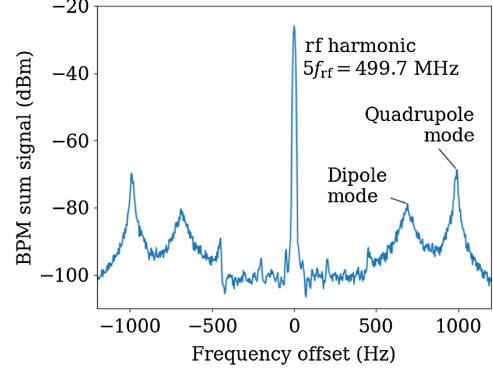
FIG. 14.   Example spectrum-analyzer measurement of the coherent dipole and quadrupole Robinson modes from sidebands of the fifth rf harmonic.

deliver an approximately quartic potential at a Landau voltage of 190 kV given the machine parameters. The advantage of performing the experiment at as low a current as possible is that the beam is less unstable due to HOM-driven coupled-bunch modes and Robinson-mode coupling (as discussed below), which may interfere with measurements of the modes of interest.

The results are shown in Fig. 15 and are compared with the predictions of the theory presented in [8].
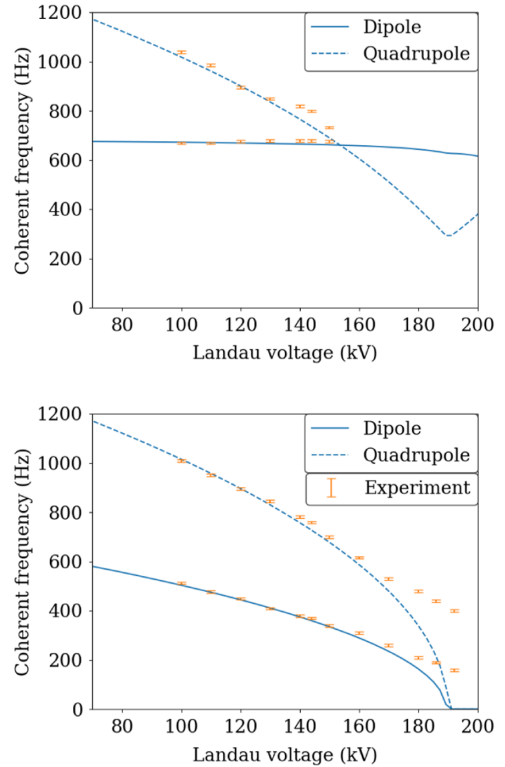
FIG. 15.   Measurements of the coherent dipole and quadrupole resonant frequencies for coupled-bunch modes 0 (top) and ± 1 (bottom) along with the theoretical predictions at 50 mA with an rf voltage of 650 kV. The errors are estimated as half the resolution bandwidth of the spectrum analyser.

As the Landau voltage is increased, the coherent frequency of the Robinson dipole mode stays roughly constant while that of the Robinson quadrupole mode decreases. At a particular Landau voltage, both modes have the same frequency and a coupling instability occurs. Although, under the theory used here which does not treat mode-coupling at all, this is at a single point, there is in reality a coupling bandwidth due to radiation damping and the tune spread within the bunches. Under the experimental conditions specified here, the mode-coupling bandwidth is small enough that the instability does not persist when flat-potential conditions are met, even without the mode-0 damper [17]. Throughout the measurement, modes ± 1 were stable but at the lowest Landau-cavity fields, other coupled-bunch modes were unstable.

The coherent frequencies of the mode-1 dipole and quadrupole modes are both reduced by the impedance. Eventually, they reach very low values but at 90 mA, no mode-1 instability occurs because of Landau damping. Nevertheless, these measurements give confidence that the origin of the mode-1 instability is not a mode coupling and no mode coupling is predicted at higher currents either where mode $+1$ is predicted to be unstable.

---

[1] P. F. Tavares, A. Andersson, A. Hansson, and J. Breunlin, Equilibrium bunch density distribution with passive harmonic cavities in a storage ring, Phys. Rev. ST Accel. Beams **17,** 064401 (2014).

[2] R. A. Bosch, K. J. Kleman, and J. J. Bisognano, Robinson instabilities with a higher-harmonic cavity, Phys. Rev. ST Accel. Beams **4,** 074401 (2001).

[3] M. Venturini, Passive higher-harmonic rf cavities with general settings and multibunch instabilities in electron storage rings, Phys. Rev. Accel. Beams **21,** 114404 (2018).

[4] T. He, W. Li, Z. Bai, and L. Wang, Periodic transient beam loading effect with passive harmonic cavities in electron storage rings, Phys. Rev. Accel. Beams **25,** 024401 (2022).

[5] P. B. Wilson and J. E. Griffin, High energy electron linacs; application to storage ring rf systems and linear colliders, AIP Conf. Proc. **87,** 450 (1982).

[6] J. Jacob, 4th harmonic rf project at the ESRF, 2020, Presented at ESLS XXVIII (2020), https://www.esrf.fr/files/live/sites/www/files/events/conferences/2020/28th%20ESLS%20Workshop/JACOB_2020-12-16%20ESLS_4HC.pptx.

[7] P. F. Tavares, S. C. Leemann, M. Sjöström, and Å. Andersson, The MAX IV storage ring project, J. Synchrotron Radiat. **21,** 862 (2014).

[8] F. J. Cullinan, A. Andersson, and P. F. Tavares, Harmonic-cavity stabilization of longitudinal coupled-bunch instabilities with a nonuniform fill, Phys. Rev. Accel. Beams **23,** 074402 (2020).

[9] K. A. Thompson and R. D. Ruth, Transverse and longitudinal coupled bunch instabilities in trains of closely spaced bunches, in *Proceedings of the 1989 IEEE Particle Accelerator Conference, Accelerator Science and Technology* (IEEE, New York, 1989), Vol. 2, pp. 792–794.

[10] T. He, Novel perturbation method for judging the stability of the equilibrium solution in the presence of passive harmonic cavities, Phys. Rev. Accel. Beams **25,** 094402 (2022).

[11] S. Krinsky and J. M. Wang, Longitudinal instabilities of bunched beams subject to a non-harmonic rf potential, Part. Accel. **17,** 109 (1985).

[12] R. R. Lindberg, Theory of coupled-bunch longitudinal instabilities in a storage ring for arbitrary rf potentials, Phys. Rev. Accel. Beams **21,** 124402 (2018).

[13] F. J. Cullinan, A. Andersson, and P. F. Tavares, Longitudinal stability with Landau cavities at MAX IV, in *Procedings of the IPAC'20* (JACoW Publishing, Geneva, Switzerland, 2021) p. 44.

[14] M. Brosi, Diagnosing collective effects in the MAX IV storage rings, presented at I.FAST, Karlsruhe (remote) (2022).

[15] P. F. Tavares, E. Al-Dmour, Å. Andersson, F. Cullinan, B. N. Jensen, D. Olsson, D. K. Olsson, M. Sjöström, H. Tarawneh, S. Thorin, and A. Vorozhtsov, Commissioning and first-year operational results of the MAXIV 3 GeV ring, J. Synchrotron Radiat. **25,** 1291 (2018).

[16] C. Thomas, G. Rehm, H. Owen, N. Wyles, S. Botchway, V. Schlott, and M. Wahl, Bunch purity measurement for diamond, Nucl. Instrum. Methods Phys. Res., Sect. A **566,** 762 (2006).

[17] D. P. McGinnis, Beam stabilization and instrumentation systems based on internet of things technology, in *Low-Level Radio Frequency Workshop* (2019) arXiv:1910.07822.

[18] Dimtel Inc., https://www.dimtel.com (2014).

[19] K. C. Harkay, T. Berenc, L. Emery, U. Wienands, D. Teytelman, J. Byrd, and R. Dowd, Characterizing the coupled bunch driving terms in a storage ring, in *Proceedings of the 6th International Beam Instrumentation Conference, IBIC 2017* (JACoW Publishing, Geneva, 2017) p. 21–27, cited by: 2.

[20] F. J. Cullinan, Review of harmonic cavities in fourth-generation storage rings, in *67th ICFA Advanced Beam Dynamics Workshop of Future Light Sources: FLS 2023* (JACoW Publishing, Geneva, 2023).

[21] See Supplemental Material at http://link.aps.org/supplemental/10.1103/PhysRevAccelBeams.27.044403 for all of the experimental results in text format.

[22] https://github.com/fracul/mode-1-maxiv.

[23] K. Y. Ng, Longitudinal coupled-bunch instabilities, in *Physics of Intensity Dependent Beam Instabilities* (World Scientific, Singapore, 2005), pp. 301–314, https://doi.org/10.1142/5835.